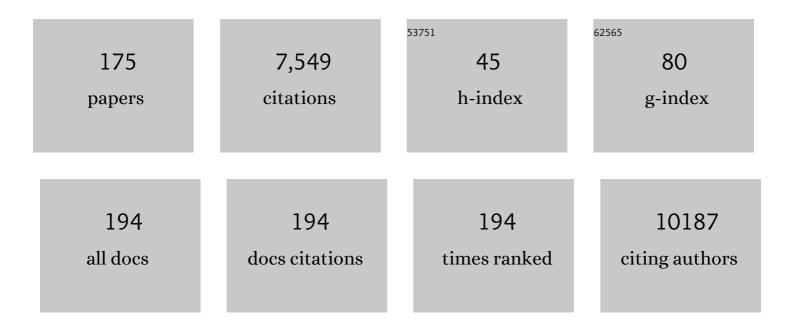
List of Publications by Year in descending order

Source: https://exaly.com/author-pdf/2502108/publications.pdf Version: 2024-02-01



#	Article	IF	CITATIONS
1	Heavy metal pollution in the soil around municipal solid waste incinerators and its health risks in China. Environmental Research, 2022, 203, 111871.	3.7	29
2	Simultaneous detection of heavy metals in solutions by electrodeposition assisted laser induced breakdown spectroscopy. Journal of Laser Applications, 2022, 34, 012021.	0.8	5
3	Technical note: Real-time diagnosis of the hygroscopic growth micro-dynamics of nanoparticles with Fourier transform infrared spectroscopy. Atmospheric Chemistry and Physics, 2022, 22, 3097-3109.	1.9	2
4	Novel application of pyrolytic carbon generated from waste tires: Hydrolytic and methanogenic performance promotion in vinegar residue anaerobic digestion. Waste Management, 2022, 143, 15-22.	3.7	3
5	Insights into the effects of micro and nanoscale FeO on elimination of excessive acidification during anaerobic digestion of the organic fraction of municipal solid waste: Similarities and differences in reactor performance and syntrophic metabolism. Fuel, 2022, 320, 123923.	3.4	9
6	Curbing dioxin emissions from municipal solid waste incineration: China's action and global share. Journal of Hazardous Materials, 2022, 435, 129076.	6.5	20
7	Three-dimensional reconstruction of a leaking gas cloud based on two scanning FTIR remote-sensing imaging systems. Optics Express, 2022, 30, 25581.	1.7	3
8	Ozone Profiles, Precursors, and Vertical Distribution in Urban Lhasa, Tibetan Plateau. Remote Sensing, 2022, 14, 2533.	1.8	3
9	Formation and Mechanism of Magnesium Titanate in the Process of Ilmenite Reduction. Mineral Processing and Extractive Metallurgy Review, 2021, 42, 162-171.	2.6	4
10	Mechanism and dynamic evolution of leachate collection system clogging in MSW landfills in China. Waste Management, 2021, 120, 314-321.	3.7	14
11	Ammonium nitrate is a risk for environment: A case study of Beirut (Lebanon) chemical explosion and the effects on environment. Ecotoxicology and Environmental Safety, 2021, 210, 111834.	2.9	12
12	Development and Application of a Wide Dynamic Range and High Resolution Atmospheric Aerosol Water-Based Supersaturation Condensation Growth Measurement System. Atmosphere, 2021, 12, 558.	1.0	0
13	Synthesis of zero-valent iron/biochar by carbothermal reduction from wood waste and iron mud for removing rhodamine B. Environmental Science and Pollution Research, 2021, 28, 48556-48568.	2.7	5
14	Development of a Laser Gas Analyzer for Fast CO2 and H2O Flux Measurements Utilizing Derivative Absorption Spectroscopy at a 100 Hz Data Rate. Sensors, 2021, 21, 3392.	2.1	5
15	Lidar vertical observation network and data assimilation reveal key processes driving the 3-D dynamic evolution of PM _{2.5} concentrations over the North China Plain. Atmospheric Chemistry and Physics, 2021, 21, 7023-7037.	1.9	16
16	Quantifying variability, source, and transport of CO in the urban areas over the Himalayas and Tibetan Plateau. Atmospheric Chemistry and Physics, 2021, 21, 9201-9222.	1.9	10
17	Ecoâ€environmental benefits analysis of EcoPartnerships program of production technology of calcium carbonate from lime mud produced by alkaline papermaking. Environmental Progress and Sustainable Energy, 2021, 40, e13697.	1.3	2
18	Mini art review for zero valent iron application in anaerobic digestion and technical bottlenecks. Science of the Total Environment, 2021, 791, 148415.	3.9	29

#	Article	IF	CITATIONS
19	Phase distribution of PCDD/Fs in flue gas from municipal solid waste incinerator with ultra-low emission control in China. Chemosphere, 2021, 276, 130166.	4.2	19
20	Reconstruction of a leaking gas cloud from a passive FTIR scanning remote-sensing imaging system. Applied Optics, 2021, 60, 9396.	0.9	7
21	Vertical profile of aerosols in the Himalayas revealed by lidar: New insights into their seasonal/diurnal patterns, sources, and transport. Environmental Pollution, 2021, 285, 117686.	3.7	11
22	Contribution of continuously stable sediment input to the formation of the Pearl River delta since the middle Holocene. Quaternary International, 2021, 598, 78-89.	0.7	3
23	The influence of mesoscale eddies on sedimentary processes in the western South China Sea since 32 kyr BP. Marine Geology, 2021, 441, 106621.	0.9	7
24	Long-term characterization and resource potential evaluation of the digestate from food waste anaerobic digestion plants. Science of the Total Environment, 2021, 794, 148785.	3.9	34
25	Fate of dioxins in a municipal solid waste incinerator with state-of-the-art air pollution control devices in China. Environmental Pollution, 2021, 289, 117798.	3.7	13
26	An active RH-controlled dry-ambient aerosol size spectrometer (DAASS) for the accurate measurement of ambient aerosol water content. Journal of Aerosol Science, 2021, 158, 105831.	1.8	2
27	Facile one-step synthesis and enhanced photocatalytic activity of a WC/ferroelectric nanocomposite. Journal of Materials Chemistry A, 2021, 9, 22861-22870.	5.2	5
28	Novel method for comprehensive utilization of MSWI fly ash through co-reduction with red mud to prepare crude alloy and cleaned slag. Journal of Hazardous Materials, 2020, 384, 121315.	6.5	62
29	Development of a static test apparatus for evaluating the performance of three PM2.5 separators commonly used in China. Journal of Environmental Sciences, 2020, 87, 238-249.	3.2	7
30	ldentifying the wintertime sources of volatile organic compounds (VOCs) from MAX-DOAS measured formaldehyde and glyoxal in Chongqing, southwest China. Science of the Total Environment, 2020, 715, 136258.	3.9	45
31	Recovery of metals from municipal solid waste incineration fly ash and red mud via a co-reduction process. Resources, Conservation and Recycling, 2020, 154, 104600.	5.3	40
32	Development and Application of HECORA Cloud Retrieval Algorithm Based On the O2-O2 477 nm Absorption Band. Remote Sensing, 2020, 12, 3039.	1.8	4
33	Concentration-Emission Matrix (CEM) Spectroscopy Combined with GA-SVM: An Analytical Method to Recognize Oil Species in Marine. Molecules, 2020, 25, 5124.	1.7	0
34	An automated dynamic chamber system for exchange flux measurement of reactive nitrogen oxides (HONO and NOX) in farmland ecosystems of the Huaihe River Basin, China. Science of the Total Environment, 2020, 745, 140867.	3.9	7
35	Validation of Water Vapor Vertical Distributions Retrieved from MAX-DOAS over Beijing, China. Remote Sensing, 2020, 12, 3193.	1.8	10
36	The BioChemical Clogging of Landfill Leachate Collection System: Based on Laboratory Studies. International Journal of Environmental Research and Public Health, 2020, 17, 2299.	1.2	4

#	Article	IF	CITATIONS
37	HCB dechlorination combined with heavy metals immobilization in MSWI fly ash by using n-Al/CaO dispersion mixture. Journal of Hazardous Materials, 2020, 392, 122510.	6.5	21
38	Anthropogenic effect on heavy metal contents in surface sediments of the Bengal Basin river system, Bangladesh. Environmental Science and Pollution Research, 2020, 27, 19688-19702.	2.7	15
39	Sea Level Change Controlled the Sedimentary Processes at the Makran Continental Margin Over the Past 13,000Âyr. Journal of Geophysical Research: Oceans, 2020, 125, e2019JC015703.	1.0	9
40	The Determination of Aerosol Distribution by a No-Blind-Zone Scanning Lidar. Remote Sensing, 2020, 12, 626.	1.8	10
41	Concentration Quantification of Oil Samples by Three-Dimensional Concentration-Emission Matrix (CEM) Spectroscopy. Applied Sciences (Switzerland), 2020, 10, 315.	1.3	5
42	Influence of temperature on enhancement of volatile fatty acids fermentation from organic fraction of municipal solid waste: Synergism between food and paper components. Bioresource Technology, 2020, 304, 122980.	4.8	37
43	Leaching behavior and potential ecological risk of heavy metals in Southwestern China soils applied with sewage sludge compost under acid precipitation based on lysimeter trials. Chemosphere, 2020, 249, 126212.	4.2	22
44	Toward separation at source: Evolution of Municipal Solid Waste management in China. Frontiers of Environmental Science and Engineering, 2020, 14, 1.	3.3	37
45	Exploring the roles of zero-valent iron in two-stage food waste anaerobic digestion. Waste Management, 2020, 107, 91-100.	3.7	49
46	Using Lidar technology to assess regional air pollution and improve estimates of PM _{2.5} transport in the North China Plain. Environmental Research Letters, 2020, 15, 094071.	2.2	15
47	A new method to determine the aerosol optical properties from multiple-wavelength O ₄ absorptions by MAX-DOAS observation. Atmospheric Measurement Techniques, 2019, 12, 3289-3302.	1.2	23
48	The effect of ISR on OFMSW during acidogenic fermentation for the production of AD precursor: kinetics and synergies. RSC Advances, 2019, 9, 18147-18156.	1.7	10
49	A novel insight into the influence of thermal pretreatment temperature on the anaerobic digestion performance of floatable oil-recovered food waste: Intrinsic transformation of materials and microbial response. Bioresource Technology, 2019, 293, 122021.	4.8	17
50	Source-to-sink processes of fluvial sediments in the northern South China Sea: Constraints from river sediments in the coastal region of South China. Journal of Asian Earth Sciences, 2019, 185, 104020.	1.0	23
51	New archive of another significant potential sediment source in the South China Sea. Marine Geology, 2019, 410, 16-21.	0.9	10
52	FeO inhibits bio-foam generating in anaerobic digestion reactor under conditions of organic shock loading and re-startup. Waste Management, 2019, 92, 107-114.	3.7	17
53	Primary and secondary sources of ambient formaldehyde in the Yangtze River Delta based on Ozone Mapping and Profiler Suite (OMPS) observations. Atmospheric Chemistry and Physics, 2019, 19, 6717-6736.	1.9	60
54	Comparison of long-term stability under natural ageing between cement solidified and chelator-stabilised MSWI fly ash. Environmental Pollution, 2019, 250, 68-78.	3.7	56

#	Article	IF	CITATIONS
55	Staged fine-grained sediment supply from the Himalayas to the Bengal Fan in response to climate change over the past 50,000 years. Quaternary Science Reviews, 2019, 212, 164-177.	1.4	21
56	Clay mineral compositions in surface sediments of the Ganges-Brahmaputra-Meghna river system of Bengal Basin, Bangladesh. Marine Geology, 2019, 412, 27-36.	0.9	44
57	Geochemistry of core sediments along the Active Channel, northeastern Indian Ocean over the past 50,000†years: Sources and climatic implications. Palaeogeography, Palaeoclimatology, Palaeoecology, 2019, 521, 151-160.	1.0	11
58	Atmosphere boundary layer height and its effect on air pollutants in Beijing during winter heavy pollution. Atmospheric Research, 2019, 215, 305-316.	1.8	79
59	Development of a field system for measurement of tropospheric OH radical using laser-induced fluorescence technique. Optics Express, 2019, 27, A419.	1.7	25
60	Leaching characteristic of toxic trace elements in soils amended by sewage sludge compost: A comparison of field and laboratory investigations. Environmental Pollution, 2018, 237, 244-252.	3.7	27
61	Enhancing syntrophic associations among Clostridium butyricum, Syntrophomonas and two types of methanogen by zero valent iron in an anaerobic assay with a high organic loading. Bioresource Technology, 2018, 257, 181-191.	4.8	48
62	Sediment provenance in the western Pacific warm pool from the last glacial maximum to the early Holocene: Implications for ocean circulation and climatic change. Palaeogeography, Palaeoclimatology, Palaeoecology, 2018, 493, 55-63.	1.0	4
63	Investigations of temporal and spatial distribution of precursors SO ₂ and NO ₂ vertical columns in the North China Plain using mobile DOAS. Atmospheric Chemistry and Physics, 2018, 18, 1535-1554.	1.9	32
64	Effect of FeO addition on volatile fatty acids evolution on anaerobic digestion at high organic loading rates. Waste Management, 2018, 71, 719-727.	3.7	72
65	Design, implementation, and evaluation of an Internet of Things (IoT) network system for restaurant food waste management. Waste Management, 2018, 73, 26-38.	3.7	124
66	Tropospheric NO ₂ , SO ₂ , and HCHO over the East China Sea, using ship-based MAX-DOAS observations and comparison with OMI and OMPS satellite data. Atmospheric Chemistry and Physics, 2018, 18, 15387-15402.	1.9	49
67	Ship-based MAX-DOAS measurements of tropospheric NO ₂ , SO ₂ , and HCHO distribution along the Yangtze River. Atmospheric Chemistry and Physics, 2018, 18, 5931-5951.	1.9	38
68	Characterization of naturally aged cement-solidified MSWI fly ash. Waste Management, 2018, 80, 101-111.	3.7	62
69	On-line analysis of algae in water by discrete three-dimensional fluorescence spectroscopy. Optics Express, 2018, 26, A251.	1.7	18
70	Phytoplankton photosynthetic rate measurement using tunable pulsed light induced fluorescence kinetics. Optics Express, 2018, 26, A293.	1.7	14
71	Development of a portable cavity ring down spectroscopy instrument for simultaneous, in situ measurement of NO3 and N2O5. Optics Express, 2018, 26, A433.	1.7	24
72	Feature issue introduction: light, energy and the environment, 2017. Optics Express, 2018, 26, A636.	1.7	3

#	Article	IF	CITATIONS
73	Full-circle range and microradian resolution angle measurement using the orthogonal mirror self-mixing interferometry. Optics Express, 2018, 26, 10371.	1.7	37
74	Study on baseline correction methods for the Fourier transform infrared spectra with different signal-to-noise ratios. Applied Optics, 2018, 57, 5794.	0.9	18
75	The Physical Clogging of the Landfill Leachate Collection System in China: Based on Filtration Test and Numerical Modelling. International Journal of Environmental Research and Public Health, 2018, 15, 318.	1.2	19
76	Dechlorination of Hexachlorobenzene in Contaminated Soils Using a Nanometallic Al/CaO Dispersion Mixture: Optimization through Response Surface Methodology. International Journal of Environmental Research and Public Health, 2018, 15, 872.	1.2	16
77	Mercaptopropionic acid-capped Mn-doped ZnS quantum dots and Pb2+ as sensing system for rapid and sensitive room-temperature phosphorescence detection of sulfide in water. Journal of Photochemistry and Photobiology A: Chemistry, 2018, 364, 88-96.	2.0	6
78	Temporal and spatial patterns of sediment deposition in the northern South China Sea over the last 50,000 years. Palaeogeography, Palaeoclimatology, Palaeoecology, 2017, 465, 212-224.	1.0	41
79	Greenhouse gas emissions from municipal solid waste with a high organic fraction under different management scenarios. Journal of Cleaner Production, 2017, 147, 451-457.	4.6	56
80	Release of heavy metals during long-term land application of sewage sludge compost: Percolation leaching tests with repeated additions of compost. Chemosphere, 2017, 169, 271-280.	4.2	81
81	Environmental performance evaluation of different municipal solid waste management scenarios in China. Resources, Conservation and Recycling, 2017, 125, 98-106.	5.3	114
82	Greenhouse gas emissions from different municipal solid waste management scenarios in China: Based on carbon and energy flow analysis. Waste Management, 2017, 68, 653-661.	3.7	74
83	Short-term pre-aeration applied to the dry anaerobic digestion of MSW, with a focus on the spectroscopic characteristics of dissolved organic matter. Chemical Engineering Journal, 2017, 313, 1222-1232.	6.6	19
84	Investigating the performance of a greenhouse gas observatory in Hefei, China. Atmospheric Measurement Techniques, 2017, 10, 2627-2643.	1.2	44
85	Industrial SO ₂ emission monitoring through a portable multichannel gas analyzer with an optimized retrieval algorithm. Atmospheric Measurement Techniques, 2016, 9, 1167-1180.	1.2	3
86	Sedimentary responses to sea-level rise and Kuroshio Current intrusion since the Last Glacial Maximum: Grain size and clay mineral evidence from the northern South China Sea slope. Palaeogeography, Palaeoclimatology, Palaeoecology, 2016, 450, 111-121.	1.0	31
87	Aging of solidified/stabilized electrolytic manganese solid waste with accelerated carbonation and aging inhibition. Environmental Science and Pollution Research, 2016, 23, 24195-24204.	2.7	7
88	Effects of high-pressure extruding pretreatment on MSW upgrading and hydrolysis enhancement. Waste Management, 2016, 58, 81-89.	3.7	19
89	Effects of aerobic and anaerobic biological processes on leaching of heavy metals from soil amended with sewage sludge compost. Waste Management, 2016, 58, 324-334.	3.7	25
90	Morphology characteristics and mode of CaO encapsulation during treatment of electrolytic manganese solid waste. Environmental Science and Pollution Research, 2016, 23, 21861-21871.	2.7	6

#	Article	IF	CITATIONS
91	Targeted modification of organic components of municipal solid waste by short-term pre-aeration and its enhancement on anaerobic degradation in simulated landfill bioreactors. Bioresource Technology, 2016, 216, 250-259.	4.8	22
92	Inhibiting excessive acidification using zero-valent iron in anaerobic digestion of food waste at high organic load rates. Bioresource Technology, 2016, 211, 65-71.	4.8	143
93	Comparative characterization of sewage sludge compost and soil: Heavy metal leaching characteristics. Journal of Hazardous Materials, 2016, 310, 1-10.	6.5	118
94	Enhancing anaerobic digestion of high-pressure extruded food waste by inoculum optimization. Journal of Environmental Management, 2016, 166, 31-37.	3.8	42
95	Spatial and temporal variability of odorous VOC in a food waste treatment plant using hydrothermal hydrolysis and aerobic fermentation technology. Journal of Material Cycles and Waste Management, 2015, 17, 626-636.	1.6	2
96	Characterization of odorous charge and photochemical reactivity of VOC emissions from a full-scale food waste treatment plant in China. Journal of Environmental Sciences, 2015, 29, 34-44.	3.2	24
97	Realâ€ŧime in situ monitoring of poly(lactide―co â€glycolide) coating of coronary stents using electrochemical impedance spectroscopy. Journal of Biomedical Materials Research - Part B Applied Biomaterials, 2015, 103, 691-699.	1.6	3
98	Characterization and solidification/stabilization of iron-ore sintering gas cleaning residue. Journal of Material Cycles and Waste Management, 2015, 17, 790-797.	1.6	3
99	Constructing a High-Efficiency MoO ₃ /Polyimide Hybrid Photocatalyst Based on Strong Interfacial Interaction. ACS Applied Materials & Interfaces, 2015, 7, 14628-14637.	4.0	97
100	Performance improvement of the open-cathode proton exchange membrane fuel cell by optimizing membrane electrode assemblies. International Journal of Hydrogen Energy, 2015, 40, 7159-7167.	3.8	27
101	<i>In Situ</i> Fabrication of Highly Conductive Metal Nanowire Networks with High Transmittance from Deep-Ultraviolet to Near-Infrared. ACS Nano, 2015, 9, 2502-2509.	7.3	65
102	Solid phase polymerization of phenylenediamine toward a self-supported FeN _x /C catalyst with high oxygen reduction activity. Chemical Communications, 2015, 51, 16707-16709.	2.2	13
103	Evaluating the impact of odors from the 1955 landfills in China using a bottom-up approach. Journal of Environmental Management, 2015, 164, 206-214.	3.8	39
104	Controllable electrophoresis deposition of TiO ₂ mesoporous spheres onto Ti threads as photoanodes for fiber-shaped dye-sensitized solar cells. RSC Advances, 2015, 5, 65005-65009.	1.7	8
105	Identification and characterization of odorous gas emission from a full-scale food waste anaerobic digestion plant in China. Environmental Monitoring and Assessment, 2015, 187, 624.	1.3	11
106	One-step growth of CoNi2S4 nanoribbons on carbon fibers as platinum-free counter electrodes for fiber-shaped dye-sensitized solar cells with high performance: Polymorph-dependent conversion efficiency. Nano Energy, 2015, 11, 697-703.	8.2	108
107	Influence of Membrane Thickness on Membrane Degradation and Platinum Agglomeration under Long-term Open Circuit Voltage Conditions. Electrochimica Acta, 2015, 153, 254-262.	2.6	35
108	Ultra-thin layer structured anodes for highly durable low-Pt direct formic acid fuel cells. Nano Research, 2014, 7, 1569-1580.	5.8	54

#	Article	IF	CITATIONS
109	Haze insights and mitigation in China: An overview. Journal of Environmental Sciences, 2014, 26, 2-12.	3.2	91
110	Studies on structural and mechanical properties under isostatic compression with large-scale discrete element simulations. Acta Mechanica Solida Sinica, 2014, 27, 129-136.	1.0	4
111	Analysis of carbon-supported platinum through potential cycling and potential-static holding. International Journal of Hydrogen Energy, 2014, 39, 13725-13737.	3.8	17
112	The degradation study of Nafion/PTFE composite membrane in PEM fuel cell under accelerated stress tests. International Journal of Hydrogen Energy, 2014, 39, 14381-14390.	3.8	103
113	Simulations of Bingham plastic flows with the multiple-relaxation-time lattice Boltzmann model. Science China: Physics, Mechanics and Astronomy, 2014, 57, 532-540.	2.0	24
114	MnO2 nanolayers on highly conductive TiO0.54N0.46 nanotubes for supercapacitor electrodes with high power density and cyclic stability. Physical Chemistry Chemical Physics, 2014, 16, 8521.	1.3	21
115	Design and synthesis of cation-functionalized ionic liquid for application as electrolyte in proton exchange membrane fuel cells. Journal of Materials Chemistry A, 2014, 2, 19275-19281.	5.2	8
116	One-dimensional assembly of TiO ₂ nanoparticles toward enhancing light harvesting and electron transport for application in dye-sensitized solar cells. RSC Advances, 2014, 4, 10519-10524.	1.7	5
117	Porous, single crystalline titanium nitride nanoplates grown on carbon fibers: excellent counter electrodes for low-cost, high performance, fiber-shaped dye-sensitized solar cells. Chemical Communications, 2014, 50, 14321-14324.	2.2	45
118	Vitamin E assisted polymer electrolyte fuel cells. Energy and Environmental Science, 2014, 7, 3362-3370.	15.6	35
119	High catalytic activity and stability of nickel sulfide and cobalt sulfide hierarchical nanospheres on the counter electrodes for dye-sensitized solar cells. Chemical Communications, 2014, 50, 4824-4826.	2.2	90
120	Intermittent microwave synthesis of nanostructured Pt/TiN–graphene with high catalytic activity for methanol oxidation. International Journal of Hydrogen Energy, 2014, 39, 16036-16042.	3.8	10
121	Impact of cation selection on proton exchange membrane fuel cell performance with trimethylethyl amide, ethylpyridinium and ethylmethyl imidazolium ionic liquid carried by poly(vinylidene fluoride) membrane as electrolyte. Journal of Power Sources, 2014, 251, 432-438.	4.0	22
122	Rapid synthesis of nitrogen-doped graphene by microwave heating for oxygen reduction reactions in alkaline electrolyte. Chinese Journal of Catalysis, 2014, 35, 509-513.	6.9	16
123	Dispersing Pt atoms onto nanoporous gold for high performance direct formic acid fuel cells. Chemical Science, 2014, 5, 403-409.	3.7	93
124	Dechlorination of hexachlorobenzene using lead–iron bimetallic particles. Chemosphere, 2013, 90, 2403-2407.	4.2	30
125	In-situ emission characteristics of odorous gases from two food waste processing plants. Journal of Material Cycles and Waste Management, 2013, 15, 510-515.	1.6	6
126	Direct NaBH4–H2O2 fuel cell based on nanoporous gold leaves. International Journal of Hydrogen Energy, 2013, 38, 10992-10997.	3.8	23

#	Article	IF	CITATIONS
127	The maximum limiting performance improved counter electrode based on a porous fluorine doped tin oxide conductive framework for dye-sensitized solar cells. Nanoscale, 2013, 5, 4951.	2.8	12
128	In situ grown vertically oriented CuInS2 nanosheets and their high catalytic activity as counter electrodes in dye-sensitized solar cells. Chemical Communications, 2013, 49, 2028.	2.2	59
129	Fiber dye-sensitized solar cells consisting of TiO2 nanowires arrays on Ti thread as photoanodes through a low-cost, scalable route. Journal of Materials Chemistry A, 2013, 1, 11790.	5.2	38
130	Application of electrical resistivity tomography to evaluate the variation in moisture content of waste during 2Âmonths of degradation. Environmental Earth Sciences, 2013, 68, 57-67.	1.3	19
131	The performance improvement of membrane and electrode assembly in open-cathode proton exchange membrane fuel cell. International Journal of Hydrogen Energy, 2013, 38, 10978-10984.	3.8	22
132	Long-term leaching behavior of phenol in cement/activated-carbon solidified/stabilized hazardous waste. Journal of Environmental Management, 2013, 115, 265-269.	3.8	17
133	Bacterial cellulose-assisted hydrothermal synthesis and catalytic performance of La2CuO4 nanofiber for methanol steam reforming. International Journal of Hydrogen Energy, 2013, 38, 10813-10818.	3.8	13
134	Versatile nanobead-scaffolded N-SnO2mesoporous microspheres: one-step synthesis and superb performance in dye-sensitized solar cell, gas sensor, and photocatalytic degradation of dye. Journal of Materials Chemistry A, 2013, 1, 524-531.	5.2	23
135	Enhanced photovoltaic performance of a dye-sensitized solar cell using graphene–TiO2 photoanode prepared by a novel in situ simultaneous reduction-hydrolysis technique. Nanoscale, 2013, 5, 3481.	2.8	89
136	Impact assessment of intermediate soil cover on landfill stabilization by characterizing landfilled municipal solid waste. Journal of Environmental Management, 2013, 128, 259-265.	3.8	13
137	Porous ZnO nanosheet arrays constructed on weaved metal wire for flexible dye-sensitized solar cells. Nanoscale, 2013, 5, 5102.	2.8	38
138	Effect of vanadium redox species on photoelectrochemical behavior of TiO2 and TiO2/WO3 photo-electrodes. Journal of Power Sources, 2012, 213, 78-82.	4.0	36
139	Determining the Biodegradability of Leachate Through XAD-8 Adsorption. Procedia Environmental Sciences, 2012, 16, 3-8.	1.3	6
140	Vertically building Zn2SnO4 nanowire arrays on stainless steel mesh toward fabrication of large-area, flexible dye-sensitized solar cells. Nanoscale, 2012, 4, 3490.	2.8	56
141	Effect of organic compositions of aerobically pretreated municipal solid waste on non-methane organic compound emissions during anaerobic degradation. Waste Management, 2012, 32, 1116-1121.	3.7	17
142	Ultrathin, Single-Crystal WO ₃ Nanosheets by Two-Dimensional Oriented Attachment toward Enhanced Photocatalystic Reduction of CO ₂ into Hydrocarbon Fuels under Visible Light. ACS Applied Materials & Interfaces, 2012, 4, 3372-3377.	4.0	332
143	Direct N2H4/H2O2 Fuel Cells Powered by Nanoporous Gold Leaves. Scientific Reports, 2012, 2, 941.	1.6	67
144	An efficient and green approach to prepare hydrophilic imidazolium ionic liquids free of halide and its effect on oxygen reduction reaction of Pt/C catalyst. International Journal of Hydrogen Energy, 2012, 37, 13167-13177.	3.8	20

#	Article	IF	CITATIONS
145	Unique Zn-doped SnO2 nano-echinus with excellent electron transport and light harvesting properties as photoanode materials for high performance dye-sensitized solar cell. CrystEngComm, 2012, 14, 6462.	1.3	64
146	Robust Hollow Spheres Consisting of Alternating Titania Nanosheets and Graphene Nanosheets with High Photocatalytic Activity for CO ₂ Conversion into Renewable Fuels. Advanced Functional Materials, 2012, 22, 1215-1221.	7.8	373
147	Fabrication of hierarchically assembled microspheres consisting of nanoporous ZnO nanosheets for high-efficiency dye-sensitized solar cells. Journal of Materials Chemistry, 2012, 22, 14341.	6.7	57
148	Cement-based solidification/stabilization of contaminated soils by nitrobenzene. Frontiers of Environmental Science and Engineering, 2012, 6, 437-443.	3.3	7
149	Experimental study of proton exchange membrane fuel cells using Nafion 212 and Nafion 211 for portable application at ambient pressure and temperature conditions. International Journal of Hydrogen Energy, 2012, 37, 4673-4677.	3.8	16
150	Study on Platinum and Copper Nanosheets Alloys Supported on Mesoporous Titanium Dioxide Doped with Carbon Black as Electrocatalysts in PEM Fuel Cells. Electroanalysis, 2012, 24, 699-706.	1.5	8
151	Effective and rapid electrochemical detection of hydrazine by nanoporous gold. Journal of Electroanalytical Chemistry, 2011, 661, 44-48.	1.9	48
152	Solar hydrogen generation from seawater with a modified BiVO4 photoanode. Energy and Environmental Science, 2011, 4, 4046.	15.6	564
153	A quick and green approach to prepare [Rmim]OH and its application in hydrophilic ionic liquid synthesis. New Journal of Chemistry, 2011, 35, 1661.	1.4	11
154	Nanoporous gold as non-enzymatic sensor for hydrogen peroxide. Electrochimica Acta, 2011, 56, 4657-4662.	2.6	206
155	Direct immobilization of Pt–Ru alloy nanoparticles on nitrogen-doped carbon nanotubes with superior electrocatalytic performance. Journal of Power Sources, 2010, 195, 7578-7582.	4.0	54
156	Pyrolysis behaviors of oil sludge based on TG/FTIR and PY-GC/MS. Frontiers of Environmental Science and Engineering in China, 2010, 4, 59-64.	0.8	3
157	Visualization of force networks in 2D dense granular materials. Frontiers of Architecture and Civil Engineering in China, 2010, 4, 109-115.	0.4	7
158	Preparation of Pt supported on WO3–C with enhanced catalytic activity by microwave-pyrolysis method. Journal of Power Sources, 2010, 195, 2633-2637.	4.0	34
159	Poisoning and regeneration of Pd catalyst in direct formic acid fuel cell. Electrochimica Acta, 2010, 55, 5024-5027.	2.6	66
160	UNDERSTANDING FORCE CHAINS IN DENSE GRANULAR MATERIALS. International Journal of Modern Physics B, 2010, 24, 5743-5759.	1.0	56
161	High Performance Cross-Linked Poly(2-acrylamido-2-methylpropanesulfonic acid)-Based Proton Exchange Membranes for Fuel Cells. Macromolecules, 2010, 43, 6398-6405.	2.2	78
162	CEMENT/ACTIVATED-CARBON SOLIDIFICATION/STABILIZATION TREATMENT OF NITROBENZENET. , 2009, , .		0

#	Article	IF	CITATIONS
163	High catalytic performance and stability of Pt/C using acetic acid functionalized carbon. Journal of Power Sources, 2009, 194, 683-689.	4.0	25
164	In situ deposition of platinum nanoparticles on bacterial cellulose membranes and evaluation of PEM fuel cell performance. Electrochimica Acta, 2009, 54, 6300-6305.	2.6	127
165	Effects of temperature on pyrolysis products of oil sludge. Frontiers of Environmental Science and Engineering in China, 2008, 2, 8-14.	0.8	18
166	Correlation study between suspended particulate matter and DOAS data. Advances in Atmospheric Sciences, 2006, 23, 461-467.	1.9	2
167	Pd electroless plated Nafion® membrane for high concentration DMFCs. Journal of Membrane Science, 2005, 259, 27-33.	4.1	37
168	Structure and chemical composition of supported Pt–Sn electrocatalysts for ethanol oxidation. Electrochimica Acta, 2005, 50, 5384-5389.	2.6	260
169	Performance Improvement in Direct Methanol Fuel Cell Cathode Using High Mesoporous Area Catalyst Support. Electrochemical and Solid-State Letters, 2005, 8, A12.	2.2	44
170	Intercomparison of NO x , SO2, O3, and aromatic hydrocarbons measured by a commercial DOAS system and traditional point monitoring techniques. Advances in Atmospheric Sciences, 2004, 21, 211-219.	1.9	14
171	FT-IR study of the microstructure of Nafion® membrane. Journal of Membrane Science, 2004, 233, 39-44.	4.1	246
172	Study of sintered stainless steel fiber felt as gas diffusion backing in air-breathing DMFC. Journal of Power Sources, 2004, 133, 175-180.	4.0	102
173	Studies on performance degradation of a direct methanol fuel cell (DMFC) in life test. Physical Chemistry Chemical Physics, 2004, 6, 134.	1.3	135
174	Novel synthesis of highly active Pt/C cathode electrocatalyst for direct methanol fuel cell. Chemical Communications, 2003, , 394-395.	2.2	226
175	Influence of electrode structure on the performance of a direct methanol fuel cell. Journal of Power Sources, 2002, 106, 364-369.	4.0	124